

# Top-Contacts-Interface Engineering for High-Performance Perovskite Solar Cell With Reducing Lead Leakage

Huan Bi, Gaoyi Han, Mengna Guo, Chao Ding, Shuzi Hayase, Hanjun Zou, Qing Shen,\* Yao Guo,\* and Wenjing Hou\*

**Though great achievements have been realized in perovskite solar cells (PSCs), there are still some thorny challenges that exist such as: 1) How to minimize the interfacial nonradiative recombination losses; 2) How to balance the power conversion efficiency (PCE) and environmental friendliness of the PSCs. Here, effective top-contacts-interface engineering is developed via using a new multi-active site Lewis base molecule named emtricitabine (FTC). Both, experimental and theoretical results confirm that a strong chemical interaction exists between FTC and  $\text{Pb}^{2+}$ . After FTC treatment, the perovskite thin film has the lower density of defect than the control film, meanwhile, the interfacial hole extraction becomes better due to the more matched energy level. Upon the FTC passivation, the PCE of the PSCs is improved from 20.83% to 22.24%. Simultaneously, the humidity stability of the PSCs is improved after the FTC modification. Last but not least, the unpackaged target film showed less lead leakage than the control film.**

## 1. Introduction

Since first reported by Miyasaka, organic-inorganic hybrid metal-halide perovskite solar cells (PSCs) have attracted more

and more attention due to their easy fabrication, low cost, tunable bandgap, high molar absorption, etc.<sup>[1–4]</sup> For a long time, perovskite is considered to be the solar material that is most likely to replace silicon. Up to now, the single-junction PSCs have achieved a certified high-power-conversion efficiency (PCE) of 25.7%.<sup>[5]</sup> However, there are still some concerns for PSCs, such as due to the rapid crystallization, an ocean of defects may be induced at the interfaces and grain boundaries (GBs) which can cause increased non-radiative recombination and poor long-term stability.<sup>[4,6–8]</sup> Therefore, a multitude of strategies have been developed to fabricate the PSCs with high PCE and long stability.<sup>[9–15]</sup> Among them, interface passivation is considered one of the most effective methods.<sup>[16–20]</sup> In addition, mismatched energy-level alignment is another reason for the loss of PCE and stability of PSCs.<sup>[21]</sup> So, interfacial engineering is very important for improving PCE and stability.

There are several interfaces in the PSCs, where the interface between the perovskite layer and hole transport layer (HTL) is one key to achieving high PCE and stable PSCs.<sup>[22–24]</sup> As we mentioned earlier, a host of defects would be generated unavoidably in perovskite films during fast crystallization. Hitherto, various strategies have been developed to modify the perovskite/HTL interface, such as inorganic modification, ionic liquid buffer layer, Lewis acid and base, and so on.<sup>[11,22–24]</sup> Among them, Lewis acid and base are considered an attractive strategy. In addition, due to the content of  $\text{FA}^+$  being very high (about 95%) in our perovskite component, the stability of the humidity is very poor. Previous works are focused on only improving the PCE or stability of the PSCs.<sup>[11]</sup> Therefore, it is urgent to develop multifunctional interface modification molecules which can both improve the PCE and stability of the PSCs.

With the proposal of “carbon neutrality,” environmental problems are becoming more and more noticeable. Although PSCs have a sea of advantages, the environmental pollution caused by lead leakage is irreversible, and it is also one of the most worrying issues. A lot of strategies have been done to avoid lead leakage, for example, gas post-treatment and device packaging.<sup>[25–28]</sup> However, due to the complex process, an army of groups direct the eyes upon it and step back. Therefore, it is hanging over one’s head to develop a simple and effective strategy to prevent the lead leakage.

H. Bi, G. Han, M. Guo, W. Hou

Institute of Molecular Science

Key Laboratory of Materials for Energy Conversion and Storage of Shanxi Province

Shanxi University

Taiyuan 030006, P. R. China

E-mail: houwenjing@sxu.edu.cn

H. Bi, C. Ding, S. Hayase, Q. Shen

Faculty of Informatics and Engineering  
The University of Electro-Communications

Tokyo 182-8585, Japan

E-mail: shen@pc.uec.ac.jp

Y. Guo

School of Materials Science and Engineering

Henan Joint International Research Laboratory of Nanocomposite Sensing Materials

Anyang Institute of Technology

Anyang 455000, P. R. China

E-mail: guoyo@ayit.edu.cn

H. Zou

Analytical and Testing Center

Chongqing University

Chongqing 401331, P. R. China

 The ORCID identification number(s) for the author(s) of this article can be found under <https://doi.org/10.1002/solr.202200352>.

DOI: 10.1002/solr.202200352

Here, a new multi-active-site Lewis base molecule named emtricitabine (FTC) is attempted to modify the interface between perovskite ( $\text{Rb}_{0.02}(\text{FA}_{0.95}\text{Cs}_{0.05})_{0.98}\text{PbI}_{2.91}\text{Br}_{0.03}\text{Cl}_{0.06}$ ) and HTL (2,2',7,7'-Tetrakis[N,N-di(4-methoxyphenyl)amino]-9,9'-spirobifluorene (Spiro-OMeTAD)). It should be noted that we have systematically optimized the experimental formulation and introduced some beneficial ions to further improve the PCE of the PSCs, such as  $\text{Cs}^+$ ,  $\text{Rb}^+$ , and  $\text{Cl}^-$ .<sup>[11]</sup> Both theoretical and experimental results prove that there indeed exists a strong chemical interaction between the multi-active sites (such as N, O, and S) of FTC and perovskite. The result shows that after being treated through FTC, the interface nonradiative recombination can be largely suppressed, which is attributed to the defects at the interface and GBs can be passivated by FTC with the multi-active sites. The optimized device has a higher open-circuit voltage ( $V_{\text{OC}}$ ), fill factor (FF), and short-circuit current ( $J_{\text{SC}}$ ) than the pristine device. Finally, the PCE was enhanced up to 22.24%, larger than that of the control device (20.83%). In addition, the champion device exhibited long-term operational

stability. What's fascinating is that after FTC modification, notorious lead leakage in water has been suppressed. Our findings represent an important step toward the development of highly efficient, long-term stable, and Eco-friendly PSCs.

## 2. Results and Discussion

The PSCs used in this work with a structure of ITO/SnO<sub>2</sub>/perovskite/Spiro-OMeTAD/Ag as displayed in Figure 1a, where multiple active sites (such as C = O, -NH<sub>2</sub>, S, and so on) of FTC were used to modify the surface of perovskite films. More clearly the chemical structure of the molecular is listed in Figure S1, Supporting Information. As the characteristic element of the FTC molecule, F was characterized by the energy-dispersive X-ray spectroscopy (EDS). As exhibited in Figure S2, Supporting Information, the results showed that the FTC molecule was evenly distributed on the surface of the perovskite film. Fourier transform infrared spectroscopy (FTIR) and X-ray

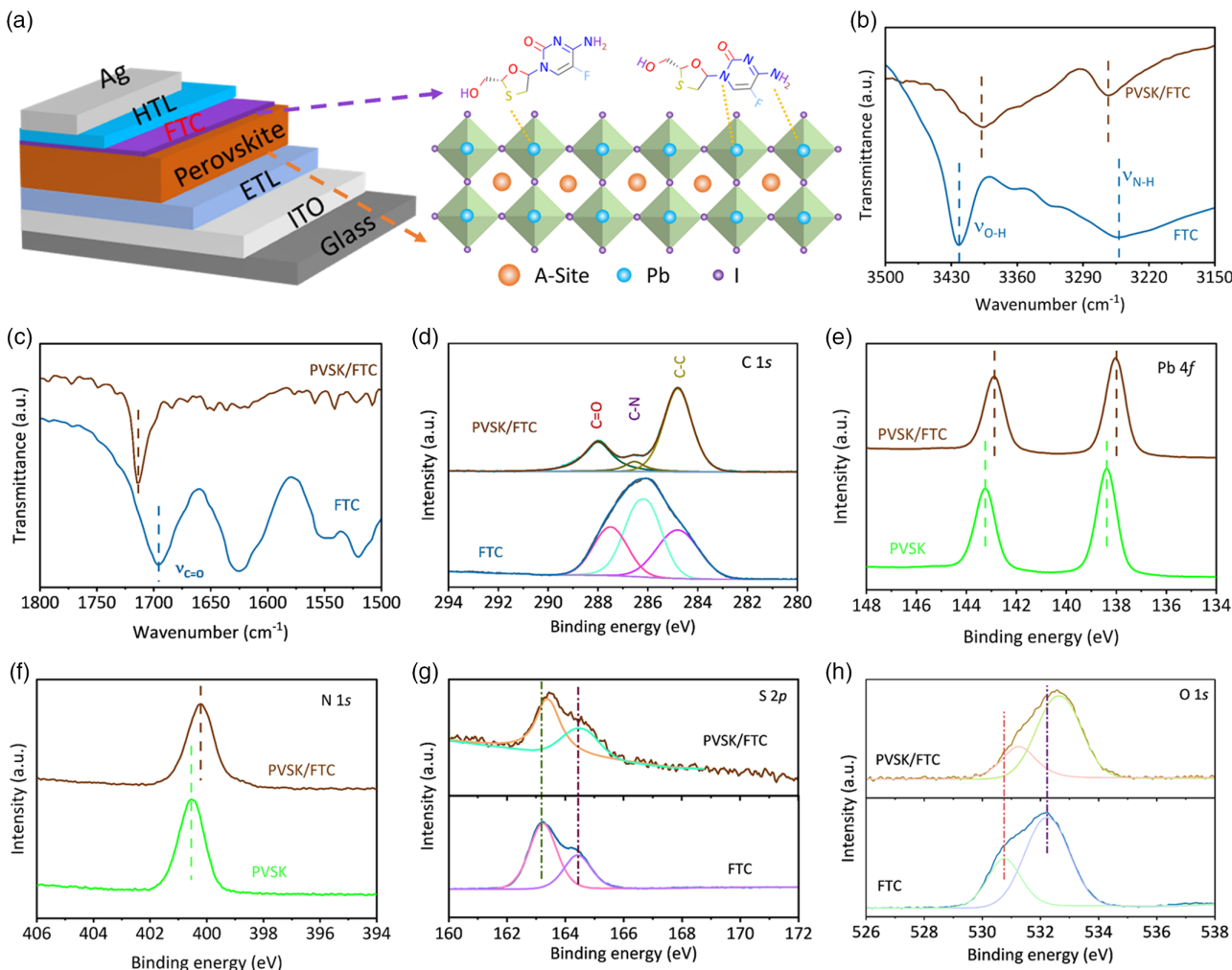


**Figure 1.** a) The device structure and schematically illustrated diagram of defect passivation by emtricitabine (FTC). b,c) Fourier transform infrared spectroscopy (FTIR) spectra of FTC and FTC-treated perovskite films. d) C 1s X-ray photoelectron spectroscopy (XPS) spectra of FTC and the perovskite films modified with FTC. e) Pb 4f and f) N 1s XPS spectra of bare perovskite film and FTC-modified perovskite film. g) S 2p and h) O 1s XPS spectra of FTC and perovskite (PVSK)/FTC thin film.

photoelectron spectroscopy (XPS) were further used to make the chemical interaction clearer between the perovskite film and the FTC. The full FTIR and XPS spectra are shown in Figure S3 and S4, Supporting Information, respectively. As shown in Figure 1b, the peaks around 3251 and 3422 cm<sup>-1</sup> belong to the stretching vibration of N–H and O–H in FTC, respectively.<sup>[29]</sup> After deposition on the perovskite (PVSF/FTC), the characteristic peaks are moved significantly ( $\nu_{N-H}$  shifts to a higher wavenumber and  $\nu_{O-H}$  moves to a lower wavenumber). Correspondingly, the peak in 1695 cm<sup>-1</sup> belonged to the stretching vibration of –C=O in FTC and also shifts to a high wavenumber after modifying the perovskite film, confirming FTC indeed chemically interacted with the perovskite film (Figure 1c).<sup>[29]</sup> Moreover, hydrogen bonding could be formed between perovskite and FTC due to there are some useful functional groups in FTC such –F and –N.<sup>[30]</sup> FTIR further gives evidence of hydrogen bonding and exhibited in Figure S5, Supporting Information, compared with bare perovskite film, the peak located at 3262 cm<sup>-1</sup> shifted to 3255 cm<sup>-1</sup> (N–H) after FTC modification.<sup>[30]</sup> As presented in Figure 1d, it is clear that the binding energy of C–N (286.17 eV) and C=O (287.51 eV) of FTC were increased to 286.54 and 287.98 eV for the perovskite film treated by FTC.<sup>[24,31]</sup> Besides, the binding energy of Pb 4f<sub>5/2</sub> (138.39 eV) and Pb 4f<sub>7/2</sub> (143.26 eV) of bare perovskite film were shifted to 138.04 and 142.90 eV for the FTC treated perovskite film, respectively (Figure 1e). This is mainly because N, O, or S in FTC contains unpaired electrons and Pb<sup>2+</sup> contains empty orbits. FTC could provide electrons to Pb<sup>2+</sup>, thus reducing the binding energy of Pb<sup>2+</sup>.<sup>[9,21,32]</sup> Figure 1f-h exhibited the XPS of N 1s (PVSF and FTC-treated PVSF), S 2p, and O 1s (FTC and PVSF/FTC thin film), it can be seen that the XPS positions of PVSF/FTC have a significant shift compared with the FTC, which further support that the strong chemical interaction between FTC and perovskite. Undoubtedly, FTIR and XPS results provide strong evidence for the chemical interactions between FTC and the perovskite film.

In addition, we have further demonstrated the strong chemical interaction between FTC and perovskite films at the theoretical level by using density functional theory (DFT) calculations. Considering the complexity of the perovskite composition of the present work, a simpler and more acceptable perovskite composition was used called FA<sub>0.92</sub>Cs<sub>0.08</sub>PbI<sub>3</sub>. Here, the defect-containing (001) heterojunction interface was constructed to verify the effect of FTC. We systematically investigated the strong interaction chemistry between FTC and perovskite. Here, the outermost perovskite layers of the inorganic layer (PbI<sub>2</sub> plane) and organic layer (formamidine hydroiodide (FAI) planes) are chosen to study, respectively. The optimized model is shown in Figure 2a. To verify the strength of chemical interaction between FTC (different contact sites) and perovskite, the binding energy ( $E_{ad}$ ) was first calculated by  $E_{ad} = [E(FTC) + E(FA_{0.91}Cs_{0.08}PbI_3) - E(FA_{0.91}Cs_{0.08}PbI_3-FTC)]/S$ , where  $E(FTC)$  is the total energies of FTC,  $E(FA_{0.91}Cs_{0.08}PbI_3)$  is the total energies of the perovskite interface,  $E(FA_{0.91}Cs_{0.08}PbI_3-FTC)$  stands for the total energies of heterojunction systems, and  $S$  is the surface area. The result can be seen in Figure 2b,c. The multiple-active sites of FTC exhibit large binding energies whether PbI<sub>2</sub> plane or FAI plane, indicating that the adsorption mode is thermodynamically most favorable and that there is a strong chemical interaction between FTC and the perovskite interface.

Charge density difference was employed to explore the chemical interaction between FTC and perovskite. Here, we choose the site O2-site in FTC (for PbI<sub>2</sub>) plane and N-site in FTC (for the FAI plane) for further study due to its highest  $E_{ad}$ . For the PbI<sub>2</sub> plane, we can see that a strong chemical interaction occurs between Pb<sup>2+</sup> and C=O (belong to FTC) (Figure S6, Supporting Information). For the FAI plane, a strong chemical interaction also occurs between Pb<sup>2+</sup> and N (belong to FTC) (Figure S7, Supporting Information). The 2D data display makes the chemical interaction clearer (Figure 2d,e). First, the (010) plane was chosen to study for the PbI<sub>2</sub> plane. As presented in Figure 2d, after FTC is modified, localized electrons are found between undercoordinated Pb and O while there is no electron density in the bare perovskite. Therefore, the charge transfer from Pb to O thus achieves a strong chemical interaction that passivates the undercoordinated Pb. In addition, Figure 2e presented the 2D data mode of the differential charge density between FTC (N-site) and perovskite when the FAI plane is located on the outermost of the perovskite surface. Changes in electron cloud density in FTC indicate that there is indeed chemical interaction between FTC (N-site) and perovskite. The density of state (DOS) still proved the strong chemical interaction between FTC and perovskite (Figure 2f and S8–S10, Supporting Information). Figure 2f presented the DOS of p belonging to the FTC and the Pb, respectively. An ocean of p orbitals overlapping indicates a strong chemical interaction between FTC and perovskite. In addition, as exhibited in Figure 2g, the peak at –1.5 eV splits into two peaks and moves toward smaller binding energy after FTC modification. Generally, lower energy indicates a more stable model structure and stronger chemical interaction. Finally, we were surprised to find that the 5p orbital of I also underwent peak splitting, which predicts that FTC also can passivate some of the cationic defects (Figure S11, Supporting Information). Up to now, we have demonstrated theoretically and experimentally that there are strong interactions between FTC and perovskite film and that these interactions can reduce the defects in perovskite and further improve the PCE of PSCs.

UV-vis absorption measurement was executed to investigate the effect of the perovskite film modified by FTC on light-harvesting property. As exhibited in Figure 3a, almost identical UV-vis absorption intensity was seen for both control and target perovskite films. Meanwhile, the bandgap of the perovskite thin film did not change after introducing the FTC (Figure S12, Supporting Information,  $E_g = 1.57$  eV). X-ray diffraction measurement (XRD) was further used to gain insights into the effect of FTC modification on the crystallinity and structure of the perovskite thin film. As shown in Figure 3b, the characteristic peaks of perovskite films that appeared at around 14.47° and 28.61° were designated as the (110) and (220), respectively.<sup>[11]</sup> The same diffraction peak position and intensity indicate that the crystal structure of perovskite was not changed after the FTC modification. In addition, the crystallinity was also not affected after modification, which was inferred from almost the same diffraction peak intensity. The top-view scanning electron microscope (SEM) images of the perovskite films are exhibited in Figure 3c,d. It can be seen that the sizes of the crystal did not change significantly whether FTC modification or not. However, some pinholes disappeared after the interface modification. All in all, though the crystal size and crystallinity of the films were

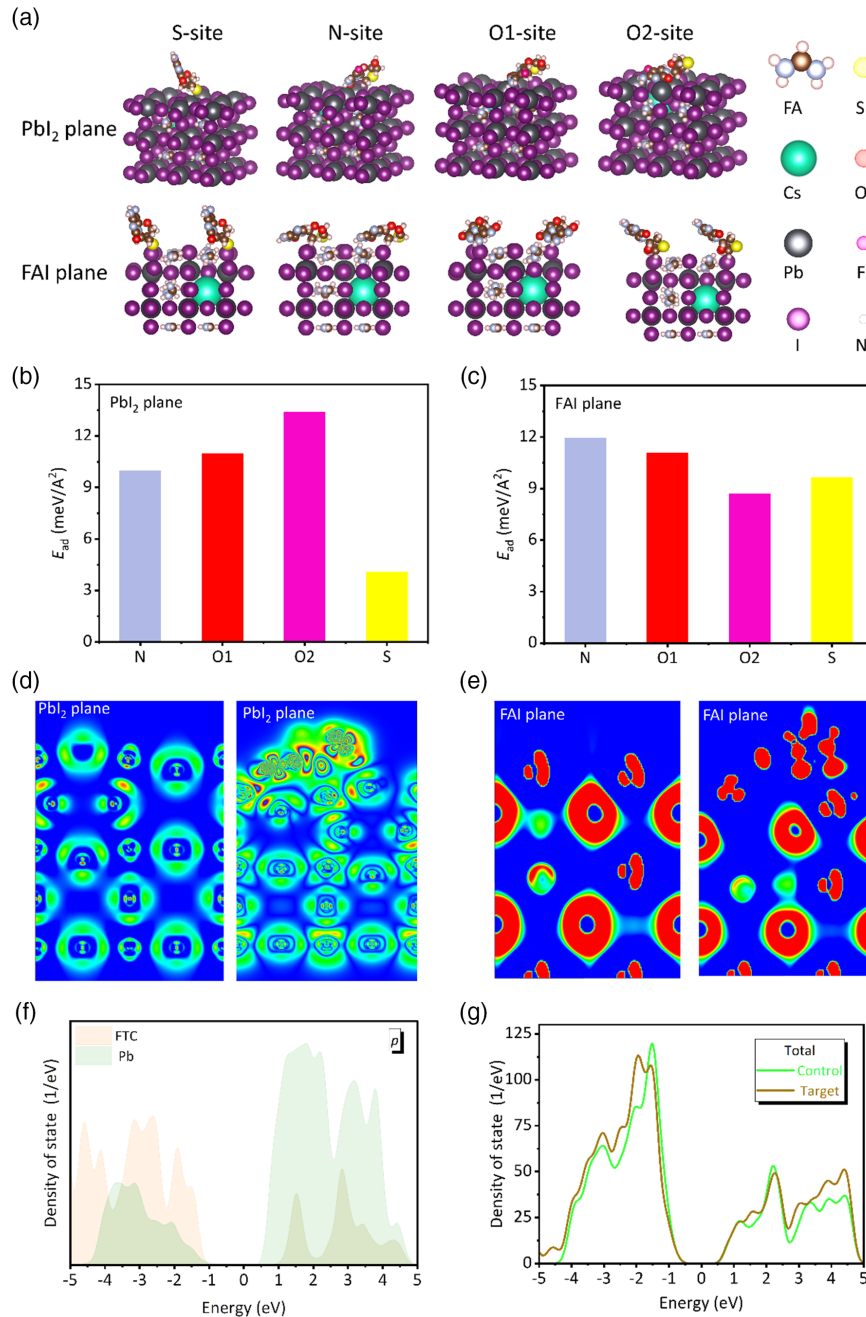


**Figure 2.** a) The interfaces for the inorganic  $\text{PbI}_2$  plane with the iodine defect in contact with the different sites of FTC molecules (top: inorganic  $\text{PbI}_2$  plane; bottom: formamidine hydroiodide (FAI) plane). The models were sites S, N, O1, and O2 in turn). The binding energy ( $E_{\text{ad}}$ ) of those ground-state structures for b)  $\text{PbI}_2$  plane and c) FAI plane. d) 2D visual charge density difference of control film and target film ( $\text{PbI}_2$  plane, O2-site) of the (010) plane section charge density difference with isovalue of  $0.005 \text{ e}^{-3} \text{ \AA}^{-3}$ . e) 2D visual charge density difference of control film and target film (FAI plane, N-site) of the (100) plane section charge density difference with isovalue of  $0.001 \text{ e}^{-3}$ . f) The density of states (DOS) of  $p$  orbitals belonging to the FTC and the Pb. g) DOS of the target (O2) and control films.

not affected by the modifier (Figure 3b), the morphology was slightly improved after the interface modification (Figure 3c,d).

To uncover the effect of the modifier on the defects and the interface charge recombination, steady-state photoluminescence (SSPL) and time-resolved photoluminescence (TRPL) were

measured by depositing the perovskite film on the glass. As presented in Figure 4a, the SSPL intensity of the FTC-treated perovskite film was much higher than that of the control perovskite film. TRPL response illustrated in Figure 4b can be fitted very well by the double exponential decay equation<sup>[33]</sup>

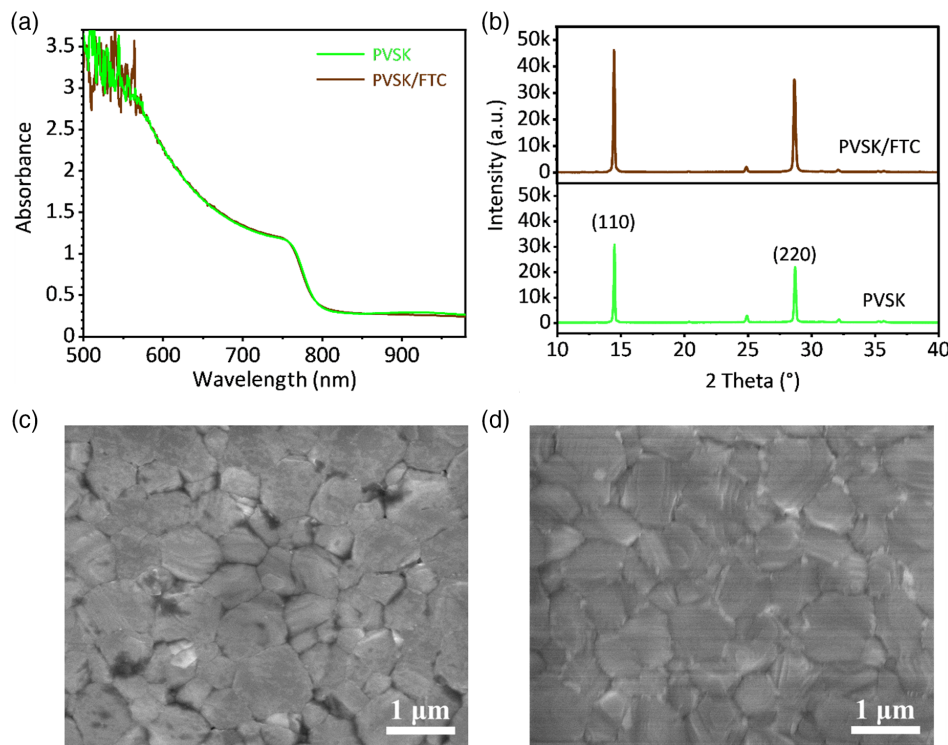


**Figure 3.** a) UV–vis absorption spectra and b) X-ray diffraction (XRD) patterns of the PVK without or with FTC treatment (PVK/FTC). c,d) Scanning electron microscope (SEM) images modified by FTC with mass concentration of 0 and 0.5 mg mL<sup>-1</sup>, respectively.

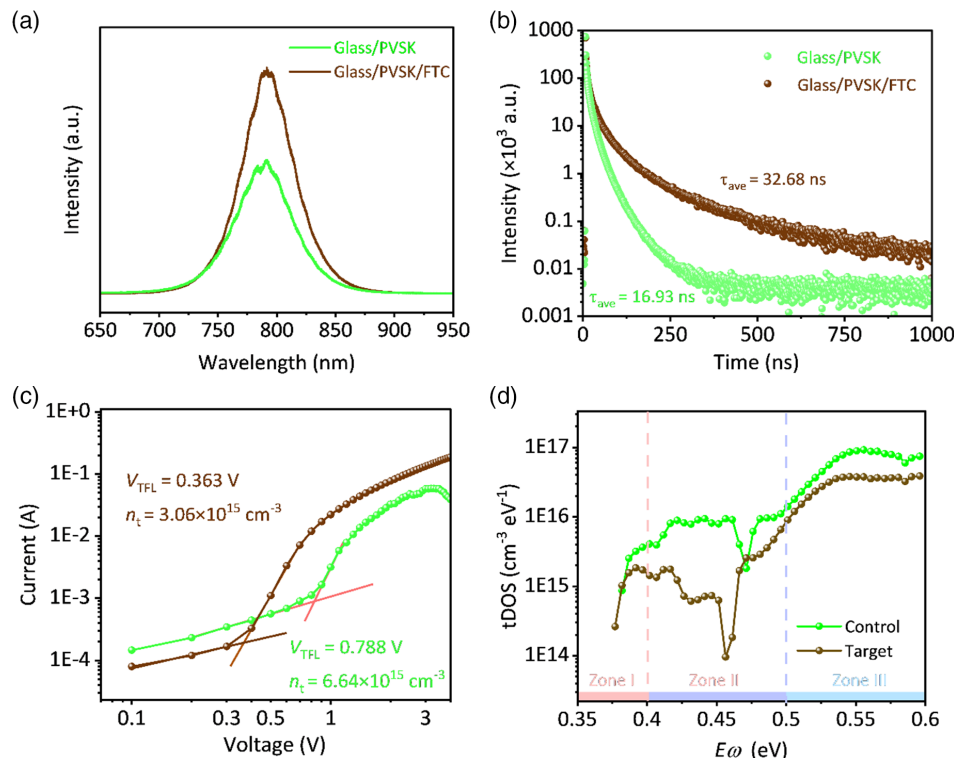


**Figure 4.** a) Steady-state photoluminescence (SSPL) and b) time-resolved PL (TRPL) of the PVK with the structures of glass/perovskite and glass/PVK/FTC, respectively. c) Dark  $I$ – $V$  curves with the structures of ITO/PVK/Au and ITO/PVK/FTC/Au, respectively. d) Trap density of states (tDOS) measurement of the control and target devices.

$$I(t) = A_1 e^{(-t/\tau_1)} + A_2 e^{(-t/\tau_2)} \quad (1)$$

And the average carrier lifetimes are calculated by the following equation<sup>[33]</sup>

$$\tau_{\text{ave}} = \frac{A_1 \tau_1^2 + A_2 \tau_2^2}{A_1 \tau_1 + A_2 \tau_2} \quad (2)$$

as shown in Table S1, Supporting Information, after modification by FTC, the average carrier lifetime increased from 16.93 to 32.82 ns (Table S1, Supporting Information). Unquestionably, the result of TRPL is in good correspondence with the SSPL. The increased PL intensity and carrier lifetimes are considered to come from the suppressed charge non-radiative recombination in the interface and GBs. This also suggests that FTC can passivate the defects (e.g., undercoordinated Pb) at the surface and GBs effectively. Space charge limited current (SCLC) measurement was further used to explore the defect densities of perovskite films without/with FTC treatment based on the structure of ITO/perovskite/(FTC)/Au.<sup>[34,35]</sup> As presented in Figure 4c, the trap-filled limit voltage ( $V_{\text{TFL}}$ ) decreased largely after the modifier was introduced (0.363 V) compared with the control film (0.788 V). The trap density of the film ( $n_t$ ) was calculated according to the following equation<sup>[36,37]</sup>

$$n_t = \frac{2\epsilon_0 \epsilon V_{\text{TFL}}}{eL^2} \quad (3)$$

where  $\epsilon_0$ ,  $\epsilon$ ,  $L$ , and  $e$  are the vacuum dielectric constant, the dielectric constant of the perovskite, the thickness of the film,

and the elementary charge, respectively. As illustrated in Figure 4c, the  $n_t$  of the film modified by FTC is  $3.06 \times 10^{15} \text{ cm}^{-3}$  while the bare film is  $6.64 \times 10^{15} \text{ cm}^{-3}$ . Further, Figure S13, Supporting Information, exhibited the SCLC test with only-hole devices (ITO/PEDOT:PSS/PVK/(FTC)/Spiro-OMeTAD/Au), the defect density of the target film ( $2.51 \times 10^{15} \text{ cm}^{-3}$ ) was less than the control film ( $4.75 \times 10^{15} \text{ cm}^{-3}$ ), reduced defect density can be attributed to the strong chemical interaction between FTC and perovskite. Thermal admittance spectroscopy (TAS) measurements were conducted to further analyze the trap density of states (TDOS) in energy space for the control and comprehensive-passivation devices. As shown in Figure 4d, there are three typical trap state bands, e.g.,  $E_0 < 0.40 \text{ eV}$  (Zone I),  $0.40 \text{ eV} < E_0 < 0.50 \text{ eV}$  (Zone II), and  $E_0 > 0.50 \text{ eV}$  (Zone III), among them, the deep trap depth regions (Zones II and III) are mainly related to the surface defects and the shallower trap-states (Zone I) are more closely related to the bulk or grain boundaries of perovskite.<sup>[38]</sup> After being modified by FTC, compared with Zone I, a more significant reduction can be seen in Zones II and III, meaning that both shallow level defects and deep level defects can be passivated and a more obvious effect in deep-level defects. Therefore, the experimental results of SSPL, TRPL, SCLC, and TAS all proved that FTC can effectively passivate the defects located in the interface and GBs via some useful groups such as carbonyl and amino groups.

Furthermore, we uncover the effect of FTC modification on the interfacial charge transfer and recombination deeply by comparing the SSPL and TRPL of the samples of glass/perovskite/Spiro-OMeTAD with and without FTC treatment. As shown in Figure 5a, the SSPL intensity of the sample is decreased after

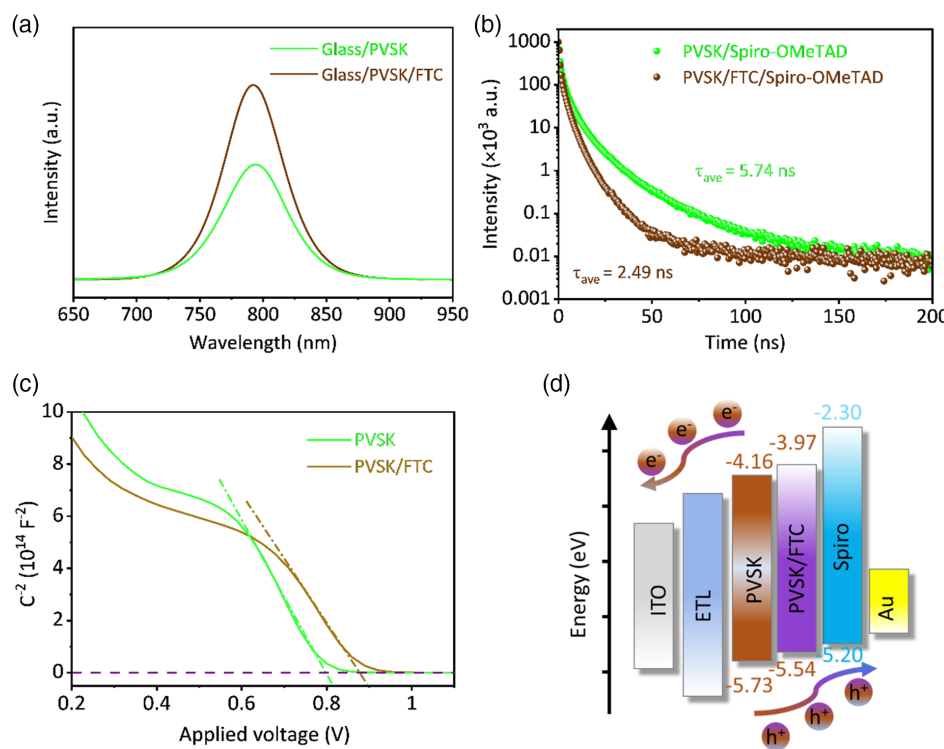


**Figure 5.** a) SSPL and b) are TRPL of the PVK with the structures of glass/perovskite/Spiro-OMeTAD and glass/perovskite/FTC/Spiro-OMeTAD, respectively. c) Mott-Schottky plots of the control and target devices. d) Energy-level diagram of device components in this work.

introducing the FTC to the interface. Corresponding with the SSPL, the TRPL results show that after the modifier is introduced, the carrier lifetime is reduced from 5.74 to 2.49 ns (Figure 5b and Table S2, Supporting Information). The carrier extraction yield ( $\gamma$ ) can be estimated via the following equation<sup>[39]</sup>

$$\gamma = \frac{\tau_{\text{ave,glass}} - \tau_{\text{ave,Spiro-OMeTAD}}}{\tau_{\text{ave,glass}}} \quad (4)$$

where  $\tau_{\text{ave,glass}}$  and  $\tau_{\text{ave,Spiro-OMeTAD}}$  stand for the average carrier lifetimes of perovskite without and with Spiro-OMeTAD deposited on the perovskite surface. The photoexcited hole extraction yield is found to be increased by 39.82% after the FTC treatment. SSPL and TRPL indicate that the interfacial carrier extraction and transfer are improved after introducing the modifier. Moreover, the ideality factor ( $n$ ) has widely been proved to be a key parameter related to the recombination of the device. Generally,  $n$  can be determined by measuring the light-intensity-dependent  $V_{\text{OC}}$  and according to the following equation<sup>[33,40]</sup>

$$V_{\text{OC}} = \frac{n k_B T}{q} \ln(J_{\text{sc}}/J_0) \quad (5)$$

where  $k_B$ ,  $T$ , and  $q$  are Boltzmann constant, absolute temperature, and elementary charge. As illustrated in Figure S14, Supporting Information, for the control device,  $n$  is 1.89 while after FTC modification,  $n$  becomes less (1.36). This indicates that FTC treatment can reduce trap-assisted nonradiative recombination in the interface and GBs. Then, the built-in potential ( $V_{\text{bi}}$ ) was got through the Mott-Schottky curve as shown in Figure 5c. The  $V_{\text{bi}}$  based on FTC-treated device is higher than that of the control device. The higher  $V_{\text{bi}}$ , the greater the driving force for the separation of photogenerated carriers is, which means that the recombination can be suppressed immensely.<sup>[10,32]</sup> Ultraviolet photoelectron spectroscopy (UPS) was carried out to uncover the deep reason why carrier extraction became better. As displayed in Figure 5d and S15 and S16, Supporting Information, the cut-off edges of the UPS spectra for the perovskite films without or with FTC modification are 17.09 and 17.42 eV, respectively. And the bandgap of perovskite is 1.57 eV calculated from the UV-vis measurement as shown in Figure S12, Supporting Information. The valence band maximum ( $E_V$ ) of the pristine perovskite and the FTC treated perovskite is  $-5.73$  and  $-5.54$  eV, respectively. The highest occupied molecular orbital (HOMO) energy level of Spiro-OMeTAD is  $-5.20$  eV. These results indicate that the  $E_V$  energy level of the FTC-treated perovskite became a better match with the HOMO of Spiro-OMeTAD, which made the transport and extraction of holes more favorable from the perovskite to the HTL.

Considering the passivated defects and improved hole extraction/transport efficiency, we attempt to modulate the mass concentration of FTC ( $0\text{--}1\text{ mg mL}^{-1}$ ) to fabricate the PSCs. The summary of the photovoltaic parameters was exhibited in Figure S17 and Table S3, Supporting Information. Figure 6a shows the  $J$ - $V$  curves of the devices treated without or with FTC at the mass concentration of  $0.5\text{ mg mL}^{-1}$ . Compared with the control device, the short circuit current ( $J_{\text{sc}}$ ), open-circuit voltage ( $V_{\text{OC}}$ ) and fill factor (FF) after modification were improved. The incident photon-to-current efficiency (IPCE) of

the device is illustrated in Figure 6b. The integrated  $J_{\text{sc}}$  value for the control device and FTC-treated one is found to be  $24.16$  and  $24.55\text{ mA cm}^{-2}$ , respectively, which is consistent with the  $J_{\text{sc}}$  got from the  $J$ - $V$  curves. We infer the reasons for the improvement of the photovoltaic parameters are as follows: 1) the fewer interface defects make less nonradiative recombination at the interfaces and the GBs, as proved by the experimental results of PL, TRPL, SCLC, and TAS (Figure 4); 2) the better-matched energy level at the perovskite/HTL interface as discussed by UPS (Figure 5d), leads to the effective holes extraction; 3) better film coverage results in the high photo-generated current and high  $J_{\text{sc}}$  (see Figure 3). In a word, all the device parameters have been improved after introducing FTC at the top contact interface.

To reveal the effect of the FTC modification on the PSCs stability, the long-term stability of the device was tested under different conditions. Unpackaged control and target devices both show excellent stability under air and humidity of 5% RH conditions (Figure 6c and S18, Supporting Information). A significant increase in PCE after aging 50 h mainly due to HTL materials needing oxygen to "activate".<sup>[41]</sup> When we put the devices under the air and humidity of 40%~45% RH condition, after 500 h, the unencapsulated target device still maintained 60.59 % of its initial PCE while the control device had almost inefficiency (Figure 6d and S19, Supporting Information). In addition, a reference modifier named lamivudine (LMD, the structure of LMD was exhibited in Figure S20, Supporting Information) was chosen to further prove the benefits of FTC owing to it having similar chemical structures to FTC. However, the missing F element differentiates the two molecules. It is well known that the F element has hydrophobic properties, so it is expected that FTC-based PSCs have better humidity stability compared to LMD-based PSCs. As presented in Figure S21, Supporting Information, after 100 h of aging, the FTC- and LMD-treated devices retain 75% and 42% of their original efficiency, respectively, while 0% for the control device when we put the unsealed devices in the 65~75% RH. Such an obvious advantage of the target devices for the stability mainly resulted from three reasons: 1) The fewer defects in the interface and GBs after the FTC treatment can reduce the corrosion sites of water; 2) hydrophobic groups (-F) also make the corrosion of water molecules difficult; 3) there is a strong chemical interaction between FTC and perovskite whether FTC-Pb or hydrogen bond.

Finally, Pb-based PSCs have been criticized because of the notorious lead leakage, so here we test the lead leakage of the perovskite film modified without/with FTC under different conditions, as illustrated in Figure 7a-c. Recently, Zhang et al reported that the solar cell can absorb light more efficiently in the sea than that on the ground and the seawater can play a role as a heat sink, increasing the operating efficiency of PSCs.<sup>[42]</sup> However, if the lead contained in PSCs flows into the ocean, it can be fatal to marine life. So, first, the effects of the FTC treatment on the stability of the perovskite film in the seawater were confirmed and the sample color changes are shown in Figure 7a. Once the film was dropped into the seawater, the color was the same, but after 20 s, the target film [Figure 7a (4–5)] still kept brown while the control [(Figure 7a (1–2))] became yellow completely, which suggests that the latter one was completely decomposed into  $\text{PbI}_2$ . And after 300 s, the control film almost

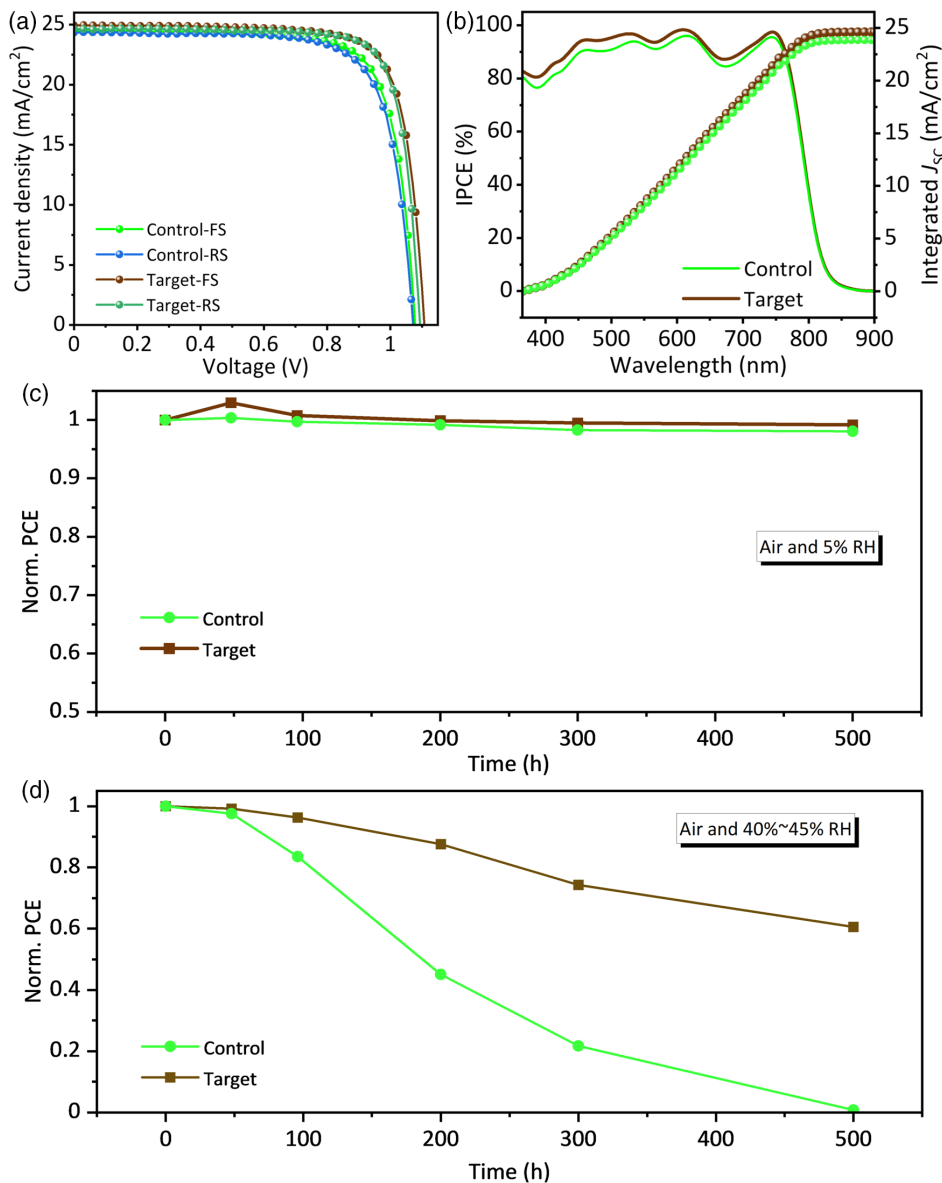


**Figure 6.** a) J-V curves and b) corresponding incident photon-to-current efficiency (IPCE) spectra of the best-performing devices based on perovskite and FTC-modified perovskite. Normalized PCE as a function of time for the unencapsulated devices without and with FTC modification aged at: c) air and humidity of 5% RH and d) air and humidity of 40–45% RH. (FS: Forward scanning; RS: Reverse scanning).

completely dissolved in seawater, but the FTC treated one was yellow. This result proved that the FTC can effectively prevent the lead leakage. Then, the solubility of the film in deionized water was tested as displayed in Figure 7b, after 300 s, both the FTC-treated film and untreated film were dissolved into the water while the control film [Figure 7b (1–3)] seemed more serious than the target film [Figure 7b (4–6)]. Finally, considering that the device can be used outdoors, some extreme situations must be taken into account, such as acidic rain. Here, combined with the local environmental conditions, we configured a certain acid solution ( $H_2SO_4$  (98%): $HNO_3$  (68%) = (8:1, *n:n*), with the pH = 5.6) to simulate the acidic rain. As shown in Figure 7c, both the control [Figure 7c (1–3)] and target [Figure 7c (4–6)] films

show good corrosion resistance. But we notice that after 20 s, the film treated by FTC still showed brown (Figure 7c-5) while the control film became yellow (Figure 7c-2) completely. An interesting phenomenon was observed that the Pb leakage became weaker in the acid solution than in deionized water, which is mainly due to the that  $SO_4^{2-}$  can react with  $Pb^{2+}$  as reported and thus slow down the dissolution of Pb in acid rain<sup>[43,44]</sup>. To further estimate the concentration of  $Pb^{2+}$  ions leaked from the perovskite to the water, the inductively coupled plasma mass spectrometry (ICP-MS) measurements were performed and the results are displayed in Figure 7d. As expected, the lead concentration in the water containing the degraded control device reaches 7.20 mg L<sup>-1</sup> (deionized water), 8.72 mg L<sup>-1</sup>

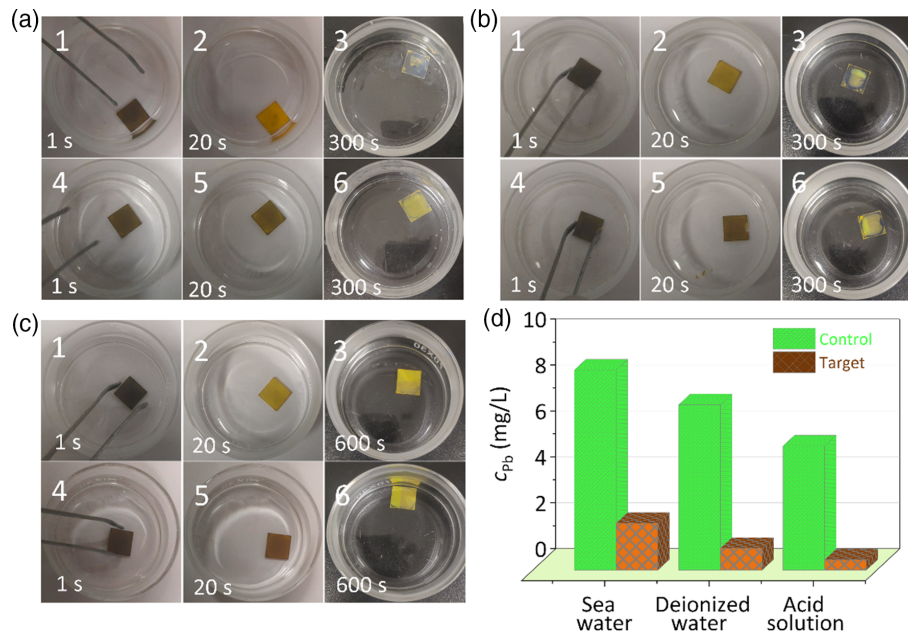


**Figure 7.** The pictures of: a) seawater, b) deionized water, and c) acid solution test on both the pristine perovskite and FTC-treated films. Note that the pH value of deionized water was adjusted to about 5.6 to simulate acidic rain conditions. d) The Pb concentration under different conditions was measured by inductively coupled plasma mass spectrometry (ICP-MS). Photo credit: Huan Bi, The University of Electro-Communication.

(seawater), and  $5.40 \text{ mg L}^{-1}$  (acid solution) at room temperature, indicating serious lead leakage. While in the water containing the FTC modified perovskite films, the deionized water, seawater, and acid solution, the Pb concentration decreased significantly by  $0.95$ ,  $2.04$ ,  $0.45 \text{ mg L}^{-1}$ , respectively.  $\text{PbI}_2$  was further employed to evaluate the FTC's ability to suppress lead leakage. As presented in Figure S22, Supporting Information. We soaked  $\text{PbI}_2$  thin film without and with FTC modification in water, and after 5 minutes we tested the lead concentration in water. Significant lead leak suppression also can be observed when we taste in  $\text{PbI}_2$ . The ultra-low lead leakage of the film is attributed to the strong chemical interaction between FTC and  $\text{Pb}^{2+}$  ions in the perovskite film surface as shown in Figure 1 and 2. Therefore, the developed FTC-modified surface can not only improve the performance and stability of the device but also can reduce the leakage of lead.

### 3. Conclusions

In summary, we have developed a multifunctional passivation strategy by introducing a multi-active site Lewis base molecule name emtricitabine (FTC) at the top contact surface of a normal structure device for achieving high PCE, stability, and environment-friendly PSCs. Both experimental and theoretical results show that the multiple active sites in FTC can chemically interact with the undercoordinated  $\text{Pb}^{2+}$  defects at the surface or GBs of perovskite films. Systematic experimental studies also proved that FTC can not only passivate the defects located in the interface and GBs but also can improve the holes extraction and transfer. TAS further reveals that the trap density of states in energy space was reduced after the FTC treatment. Finally,

the champion device achieves a high PCE of 22.24%. Meanwhile, the target device showed relatively environmentally friendly due to their low lead leakage after FTC modification. In conclusion, our results not only provide a direction for the study of high PCE and stable PSCs but also provide a reference for the preparation of environmentally friendly PSCs.

### 4. Experimental Section

**Materials:**  $\text{SnO}_2$  colloidal solution (15 wt% in water) was brought from Alfa Aesar. Lead (II) bromide ( $\text{PbBr}_2$ , 99.9%), FAI (99.9%), bis(trifluoromethane) sulfonamide lithium salt (Li-TFSI, 99%), Spiro-OMeTAD (99.86%), and 4-tert-butyl pyridine (tBP, 99%) were purchased from Advanced Election Technology CO. Ltd. Lead (II) iodide ( $\text{PbI}_2$ , 99.99%), methylammonium bromide (MABr, 99.9%), lead (II) chloride ( $\text{PbCl}_2$ , 99.99%), and methylamine hydrochloride (MACl, 99.5%) were purchased from Xi'an Polymer Light Technology Corp. Cesium iodide ( $\text{CsI}$ , 99.99%) and rubidium iodide ( $\text{RbI}$ ) were obtained from Aladdin. Acetonitrile (ACN, 99.8%) was got from Macklin. Emtricitabine (FTC, >98.0%) and lamivudine (LMD, >98.0%) were purchased from Tokyo Chemical Industry Co. Ltd. (TCI). Chlorobenzene (CB, >99.9% purity), N, N-dimethylformamide (DMF, 99.8%) and dimethyl sulfoxide (DMSO, 99.8%) were purchased from Sigma-Aldrich. All the chemicals were used without further purification.

**Device Fabrication:** Laser-patterned ITO glasses (purchased from Jiangsu Yanchang Sunlait New Energy Co., Ltd.,  $7\text{--}9 \Omega \text{ square}^{-1}$ ) were ultrasonically cleaned with detergent water and ethanol for 20 min in sequence. After being blown dry by nitrogen (99.99%), the ITO was treated with ultraviolet ozone ( $\text{UV-O}_3$ ) for 30 min. Then, the  $\text{SnO}_2$  colloidal solution was prepared by mixing the  $\text{SnO}_2$  solution and deionized water at a volume rate of 1/3. Diluted  $\text{SnO}_2$  colloidal solution was spin-coated on the ITO substrates at 3000 rpm for 30 s and then the  $\text{SnO}_2$  film was annealed at  $150^\circ\text{C}$  for 30 min. After cooling down to room temperature and then treated with  $\text{UV-O}_3$  for 20 min. Then, all substrates were transferred to an argon-filled glovebox for perovskite deposition. The 1.55 M perovskite

( $\text{Rb}_{0.02}(\text{FA}_{0.95}\text{Cs}_{0.05})_{0.98}\text{PbI}_{2.91}\text{Br}_{0.03}\text{Cl}_{0.06}$ ) precursor solution was prepared by dissolving FAI of 248.16 mg, CsI of 19.73 mg, RbI of 6.58 mg, PbI<sub>2</sub> of 682.73 mg, and PbBr<sub>2</sub> of 8.53 mg PbCl<sub>2</sub> of 12.74 mg, and MACl (additive) of 35 mg in the mixed solvents of DMF and DMSO ( $V_{\text{DMF}} : V_{\text{DMSO}} = 4:1$ ). The as-prepared perovskite precursor solution was filtered by the 0.22  $\mu\text{m}$  poly tetra fluoroethylene filter before use. The perovskite film was deposited by the consecutively spin-coating process at 4000 rpm for 30 s, where 80  $\mu\text{L}$  CB antisolvent was dripped on perovskite films at 16 s before ending the program, and the film was then annealed at 130 °C for 30 min. For FTC treatment, different mass concentrations of FTC (0, 0.25, 0.5, 0.75, and 1 mg mL<sup>-1</sup>) were dissolved in isopropyl alcohol, and then 40  $\mu\text{L}$  of FTC was spin-coated onto the perovskite film at a speed of 6000 rpm for 30 s (room temperature and without further annealing). The Spiro-OMeTAD solution was prepared by mixing 72.3 mg Spiro-OMeTAD, 28.8  $\mu\text{L}$  of tBP and 17.5  $\mu\text{L}$  Li-TFSI stock solution (520 mg Li-TFSI in 1 mL acetonitrile) in 1 mL CB. Subsequently, 20  $\mu\text{L}$  Spiro-OMeTAD solution was spin-coated onto the perovskite films at 4000 rpm for 30 s to form the hole transport layer. Finally, about 100 nm metal counter electrode was thermally evaporated on the top of Spiro-OMeTAD film under a vacuum of  $3 \times 10^{-3}$  Pa through using a shadow mask.

Lead leakage test: Seawater test by mixing NaCl (26.518 mg), MgSO<sub>4</sub> (3.305 mg), MgCl<sub>2</sub> (2.447 mg), CaCl<sub>2</sub> (1.141 mg), KCl (0.725 mg), NaHCO<sub>3</sub> (0.202 mg), and NaBr (0.083 mg) into detergent water.

**Characterization:** J-V curves were obtained using a solar simulator equipped and a Keithley 2400 source meter, and the black metal mask was employed to define the effective active area of the device to be 0.1 cm<sup>2</sup>. The PCE of the PSCs was tested under air conditions. FTIR spectroscopy was obtained on an FTIR spectrometer (Tensor27, BRUKER, Germany). UV-vis spectra were measured on an Agilent 8453 UV-vis G1103A spectrometer. Steady-state photoluminescence (SSPL) was recorded by a Confocal Raman system (iHR 550 HORIBA) with a laser of 532 nm. XPS spectra were collected from a Physical Electronics Model 5700 XPS instrument, and the data was analyzed and processed by Thermo Avantage (v5.9921) software. SEM observations were performed on SEM (FESEM, JEOL-JSM-6701 F, 7 kV) in ADD mode. The structure and crystallization of the film were characterized by using an X-ray diffractometer (D2 PHASER Desktop XRD, BRUKER, Germany). UPS was performed by PHI 5000 VersaProbe III with He I source (21.22 eV) under an applied negative bias of 9.0 V. The EDS measurement was carried out on a field emission scanning electron microscope (JEM-7900 F, Japan) with EDS equipment. The Pb concentration was detected by an ICP-MS instrument (NEXION 350, PerkinElmer). Time-resolved photoluminescence (TRPL) was measured by using a self-built scanning confocal system based on an inverted microscope (Nikon, TE2000-U) with a 450 nm laser in the State Key Laboratory of Quantum Optics and Quantum Optics Devices of Shanxi University. TAS measurements were performed by an electrochemical workstation (CHI 660e).

## Supporting Information

Supporting Information is available from the Wiley Online Library or from the author.

## Acknowledgements

This work was financially supported by the National Natural Science Foundation of China (U21A20172, 61804091, and U21A6004), Scientific and Technological Innovation Programs of Higher Education Institutions in Shanxi (2020L0002), and the Natural Science Foundation of Shanxi Province under Grant (201901D211127), Program of State Key Laboratory of Quantum Optics and Quantum Optics Devices (No: KF201910). The authors are grateful for the Scientific Research Start-up Funds of Shanxi University, and the Hundred Talents Plan of Shanxi Province. This research was partly supported by the Japan Science and Technology Agency (JST) Mirai program

(JPJMI17EA). The authors also would like to thank Shiyanjia Lab for the support of XPS and UPS tests.

## Conflict of Interest

The authors declare no conflict of interest.

## Author Contributions

H.B. and W.H. conceived the idea and designed the experiments. H.B. fabricated the devices and conducted the characterization. H.B., G.H., C.D., M.G., H.Z., Q.S., and Y.G. participated in data analysis and discussion. Y.G. Q.S. and H.B. carried out the simulation calculation and analysis. H.B., Q.S., S.H., and W.H. wrote the article, and all authors reviewed the article. Q.S. and W.H. supported and supervised the whole project.

## Data Availability Statement

Research data are not shared.

## Keywords

environment-friendly devices, MA-free perovskite solar cells, multi-active-site passivation, reducing lead leakage, surface design

Received: April 21, 2022

Revised: May 25, 2022

Published online: June 9, 2022

- [1] A. Kojima, K. Teshima, Y. Shirai, T. Miyasaka, *J. Am. Chem. Soc.* **2009**, *131*, 6050.
- [2] N. Li, X. Niu, Q. Chen, H. Zhou, *Chem. Soc. Rev.* **2020**, *49*, 8235.
- [3] N. Yang, C. Zhu, Y. Chen, H. Zai, C. Wang, X. Wang, H. Wang, S. Ma, Z. Gao, X. Wang, J. Hong, Y. Bai, H. Zhou, B.-B. Cui, Q. Chen, *Energy Environ. Sci.* **2020**, *13*, 4344.
- [4] R. Zhao, L. Xie, R. Zhuang, T. Wu, R. Zhao, L. Wang, L. Sun, Y. Hua, *ACS Energy Lett.* **2021**, *12*, 4209.
- [5] <https://www.nrel.gov/pv/cell-efficiency.html>, NREL, access.
- [6] F. Zhang, K. Zhu, *Adv. Energy Mater.* **2020**, *10*, 1902579.
- [7] D. Bi, C. Yi, J. Luo, J.-D. Décoppet, F. Zhang, S. M. Zakeeruddin, X. Li, A. Hagfeldt, M. Grätzel, *Nat. Energy* **2016**, *1*, 16142.
- [8] F. X. Xie, D. Zhang, H. Su, X. Ren, K. S. Wong, M. Grätzel, W. C. H. Choy, *ACS Nano* **2015**, *9*, 639.
- [9] H. Bi, X. Zuo, B. Liu, D. He, L. Bai, W. Wang, X. Li, Z. Xiao, K. Sun, Q. Song, Z. Zang, J. Chen, *J. Mater. Chem. A* **2021**, *9*, 3940.
- [10] X. Zuo, B. Kim, B. Liu, D. He, L. Bai, W. Wang, C. Xu, Q. Song, C. Jia, Z. Zang, D. Lee, X. Li, *Chem. Eng. J.* **2021**, *1*, 133209.
- [11] B. Liu, H. Bi, D. He, L. Bai, W. Wang, H. Yuan, Q. Song, P. Su, Z. Zang, T. Zhou, J. Chen, *ACS Energy Lett.* **2021**, *6*, 2526.
- [12] Y. Zhao, P. Zhu, M. Wang, S. Huang, Z. Zhao, S. Tan, T. H. Han, J. W. Lee, T. Huang, R. Wang, J. Xue, D. Meng, Y. Huang, J. Marian, J. Zhu, Y. Yang *Adv. Mater.* **2020**, *32*, 1907769.
- [13] Y. Yang, T. Chen, D. Pan, J. Gao, C. Zhu, F. Lin, C. Zhou, Q. Tai, S. Xiao, Y. Yuan, Q. Dai, Y. Han, H. Xie, X. Guo, *Nano Energy* **2020**, *67*, 104246.
- [14] M. A. Ruiz-Preciado, D. J. Kubicki, A. Hofstetter, L. McGovern, M. H. Futscher, A. Ummadisingu, R. Gershoni-Poranne, S. M. Zakeeruddin, B. Ehrler, L. Emsley, J. V. Milic, M. Grätzel, *J. Am. Chem. Soc.* **2020**, *142*, 1645.

- [15] Y. H. Lin, N. Sakai, P. Da, J. Wu, H. C. Sansom, A. J. Ramadan, S. Mahesh, J. Liu, R. D. J. Oliver, J. Lim, L. Aspitarte, K. Sharma, P. K. Madhu, A. B. Morales-Vilches, P. K. Nayak, S. Bai, F. Gao, C. R. M. Grovenor, M. B. Johnston, J. G. Labram, J. R. Durrant, J. M. Ball, B. Wenger, B. Stannowski, H. J. Snaith, *Science* **2020**, *369*, 96.
- [16] M. Salado, M. Andresini, P. Huang, M. T. Khan, F. Ciriaci, S. Kazim, *Adv. Funct. Mater.* **2020**, *30*, 1910561.
- [17] F. Tan, M. I. Saidaminov, H. Tan, J. Z. Fan, Y. Wang, S. Yue, X. Wang, Z. Shen, S. Li, J. Kim, Y. Gao, G. Yue, R. Liu, Z. Huang, C. Dong, X. Hu, W. Zhang, Z. Wang, S. Qu, Z. Wang, H. Sargent, *Adv. Funct. Mater.* **2020**, *30*, 2005155.
- [18] B. Wang, H. Li, Q. Dai, M. Zhang, Z. Zou, J.-L. Bredas, Z. Lin, *Angew. Chem. Int. Ed.* **2021**, *60*, 17664.
- [19] L. Wang, Q. Zhou, Y. Huang, B. Zhang, Y. Feng, *Prog. Chem.* **2020**, *32*, 119.
- [20] Z. Wang, T. Wu, L. Xiao, P. Qin, X. Yu, L. Ma, L. Xiong, H. Li, X. Chen, Z. Wang, T. Wu, L. Xiao, P. Qin, X. Yu, L. Ma, L. Xiong, H. Li, X. Chen, *J. Power Sources* **2021**, *488*, 229451.
- [21] J. Chen, N. G. Park, *Adv. Mater.* **2019**, *31*, 1803019.
- [22] Q. Jiang, Z. Ni, G. Xu, Y. Lin, P. N. Rudd, R. Xue, Y. Li, Y. Li, Y. Gao, J. Huang, *Adv. Mater.* **2020**, *32*, 2001581.
- [23] J. J. Yoo, S. Wieghold, M. C. Sponseller, M. R. Chua, S. N. Bertram, N. T. P. Hartono, J. S. Tresback, E. C. Hansen, J.-P. Correa-Baena, V. Bulović, T. Buonassisi, S. S. Shin, M. G. Bawendi, *Energy Environ. Sci.* **2019**, *12*, 2192.
- [24] Q. Jiang, Y. Zhao, X. Zhang, X. Yang, Y. Chen, Z. Chu, Q. Ye, X. Li, Z. Yin, J. You, *Nat. Photonics* **2019**, *13*, 460.
- [25] H. Zhang, K. Li, M. Sun, F. Wang, H. Wang, A. K. Y. Jen, *Adv. Energy Mater.* **2021**, *11*, 2102281.
- [26] X. Meng, X. Hu, Y. Zhang, Z. Huang, Z. Xing, C. Gong, L. Rao, H. Wang, F. Wang, T. Hu, L. Tan, Y. Song, Y. Chen, *Adv. Funct. Mater.* **2021**, *31*, 2106460.
- [27] B. Chen, C. Fei, S. Chen, H. Gu, X. Xiao, J. Huang, *Nat. Commun.* **2021**, *12*, 5859.
- [28] Y. Jiang, L. Qiu, E. J. Juarez-Perez, L. K. Ono, Z. Hu, Z. Liu, Z. Wu, L. Meng, Q. Wang, Y. Qi, *Nat. Energy* **2019**, *4*, 585.
- [29] C. Shi-yun, H. Yong, Y. San-xi, G. Yong-hao, J. Hao, *J. Magn. Reson.* **2013**, *30*, 398.
- [30] N. Li, S. Tao, Y. Chen, X. Niu, C. K. Onwudinanti, C. Hu, Z. Qiu, Z. Xu, G. Zheng, L. Wang, Y. Zhang, L. Li, H. Liu, Y. Lun, J. Hong, X. Wang, Y. Liu, H. Xie, Y. Gao, Y. Bai, S. Yang, G. Brocks, Q. Chen, H. Zhou, *Nat. Energy* **2019**, *4*, 408.
- [31] G. Beamson, *J. Chem. Educ.* **1993**, *70*, A25.
- [32] H. Bi, B. Liu, D. He, L. Bai, W. Wang, Z. Zang, J. Chen, *Chem. Eng. J.* **2021**, *418*, 129375.
- [33] Z. Zhang, A. Kumar Baranwal, S. Razey Sahamir, G. Kapil, Y. Sanehira, M. Chen, K. Nishimura, C. Ding, D. Liu, H. Li, Y. Li, M. Akmal Kamarudin, Q. Shen, T. S. Ripolles, J. Bisquert, S. Hayase, *Sol. RRL* **2021**, *5*, 2100633.
- [34] H. Zhu, F. Zhang, Y. Xiao, S. Wang, X. Li, *J. Mater. Chem. A* **2018**, *6*, 4971.
- [35] H.-C. Lin, L.-Y. Chen, T.-H. Lin, *Mater. Chem. Phys.* **2021**, *259*, 124032.
- [36] P. Su, L. Bai, H. Bi, B. Liu, D. He, W. Wang, X. Cao, S. Chen, D. Lee, H. Yang, Z. Zang, J. Chen, *ACS Appl. Mater.* **2021**, *13*, 29567.
- [37] P. Su, L. Bai, H. Bi, B. Liu, S. Chen, D. Lee, H. Yang, C. Chen, Z. Zang, J. Chen, *J. Power Sources* **2021**, *506*, 230213.
- [38] F. Zhang, S. Ye, H. Zhang, F. Zhou, Y. Hao, H. Cai, J. Song, J. Qu, *Nano Energy* **2021**, *89*, 106370.
- [39] Q. Shen, Y. Ogomi, J. Chang, S. Tsukamoto, K. Kukihara, T. Oshima, N. Osada, K. Yoshino, K. Katayama, T. Toyoda, S. Hayase, *Phys. Chem. Chem. Phys.* **2014**, *16*, 19984.
- [40] K. Nishimura, M. A. Kamarudin, D. Hirotani, K. Hamada, Q. Shen, S. Iikubo, T. Minemoto, K. Yoshino, S. Hayase, *Nano Energy* **2020**, *74*, 104858.
- [41] J. Kong, Y. Shin, J. A. Röhr, H. Wang, J. Meng, Y. Wu, A. Katzenberg, G. Kim, D. Y. Kim, T.-D. Li, E. Chau, F. Antonio, T. Siboonruang, S. Kwon, K. Lee, J. R. Kim, M. A. Modestino, H. Wang, A. D. Taylor, *Nature* **2021**, *594*, 51.
- [42] H. Zhang, X. Qiao, Y. Shen, M. Wang, *J. Energy Chem.* **2015**, *24*, 729.
- [43] G. Ren, W. Han, Z. Li, C. Liu, L. Shen, W. Guo, *Sol. Energy* **2019**, *193*, 220.
- [44] C. Zhang, H. Wang, H. Li, Q. Zhuang, C. Gong, X. Hu, W. Cai, S. Zhao, J. Chen, Z. Zang, *J. Energy Chem.* **2021**, *63*, 452.